Waves in Random and Complex Media
Vol. 00, No. 00, January 2008, 1–16

RESEARCH ARTICLE

Finite Element Simulations of Multiple Scattering in Acoustic Waveguides

Eric Lunéville & Jean-Francois Mercier[a]*

[a]*Laboratoire POEMS, UMR* 2706 *CNRS/ENSTA/INRIA, ENSTA,* 32*, Boulevard Victor,* 75739 *Paris cedex* 15*, France*

(*v3.5 released April 2008*)

We develop a numerical method to characterize multiple-scattering effects in a duct. To reduce time computations, a FEM method coupled to an integral representation of the scattered pressure field, requiring the evaluation of the duct Green's function, is used, combined with the consideration of random scatterers configurations in the form of perturbed periodic arrays. This strategy reduces the mesh size and allows parallel computations. Application to the computation by an averaging process of effective transmissions are presented. When sending a plane wave, although waveguides involve modes conversion, the mean field is found to be a plane wave. A good agreement is found when comparing to analytical models, not initially designed for a duct, excepting for some frequencies, recognized to be the band gap frequencies of the underlying periodic arrays.

Keywords: multiple-scattering, acoustic waveguide, finite element, integral representation, duct Green's function, effective parameters, perturbed periodic arrays

1. Introduction

We are interested in the propagation of acoustic waves in a random heterogeneous medium confined in a waveguide. Time harmonic regime and propagation in a horizontal 2D duct with rigid boundaries are considered. We aim to determine by direct numerical simulations the coherent field obtained by averaging fields over many different realizations of disorder. Then by interpreting this coherent field as a wave propagating in an equivalent homogeneous medium, effective properties of this equivalent medium can be extracted and compared to the predictions of available multiple scattering models, initially developed for the free space propagation.

To our knowledge such study has never been made in a duct. Numerical [1] and experimental [2] works have been realized considering scatterers located in a rectangular domain while considering waves propagation in the free space. This is not the configuration considered in usual multiple scattering models where the scatterers are located in an infinite vertical slab, leading to no lateral loss of energy. Therefore the comparison of numerical or experimental results with theoretical models has to be done with caution. In time dependent regime as in [1] and [2], it is reasonable to neglect the spurious lateral loss of energy by stopping experiments at a short time. In time harmonic regime, working in a duct prevents lateral leakage of energy. Besides, contrary to the free space case, the lateral confinement in a duct

*Corresponding author. Email: jean-francois.mercier@ensta.fr

ISSN: 0278-1077 print/ISSN 1745-5049 online

DOI: 10.1080/1745503YYxxxxxxxx
http://www.informaworld.com

allows to evaluate the energy transfers: the reflected and transmitted energies by the heterogeneous medium. In particular, when analyzing the transmitted energy, it is possible to compare the energy lost by averaging (thus carried by the incoherent field) to the energy simply reflected. Also satisfaction of energy conservation is a good test of the validity of the numerical method.

Analytical methods to deal with multiple scattering provide parameters of an effective medium equivalent to the real heterogeneous medium. The usual result is a formula for the effective wavenumber k_{eff}. A popular method ([3–7] among many others) to derive such result is to use eigenfunction expansion to describe the field sent by one scatterer to another one. In 2D cases, Bessel functions are commonly used which has the advantage to lead to semi-analytical method but restrict the study to circular obstacles. We have chosen a finite element method allowing to consider any shape of the scatterers. Since to our knowledge there is no analytical model providing the effective wavenumber in a duct, our numerical experiments provide a way to determine if the formula for effective wavenumber derived in the free space [3, 6] can be used for a duct.

In various application domains, finite element methods have been developed to study multiple scattering: propagation in unidirectional fiber-reinforced composites [7], determination of the elastic constants of a set of spheres randomly embedded in an isotropic elastic matrix [8]. In all these works, only one realization of disorder is considered. As we are interested in coherent fields, a fast numerical method is required. A method reducing the mesh to small domains surrounding each scatterers is used, coupling finite element with the integral representation of the scattered field. The Green's function of the duct is required to evaluate such integral. To reduce time computations, a random array of scatterers is built as a perturbed periodic array. It allows to split the mesh in several slices, to parallelize computations and the field in the whole domain is then obtained using a scattering matrices method. An alternative time-efficient method is to use a fast multiple method [9].

Our work is closely related to [10]. They have developed a numerical procedure for multiple wave scattering in unidirectional fiber-reinforced composite materials. They have studied time-harmonic propagation for periodic and random fiber arrangements. They have shown that the transmission coefficient of the random composite is well reproduced using the effective wavenumber predicted by a generalized self-consistent scattering model [11].

The main analogy with our work lies in the way the whole composite is constructed. They consider a semi-periodic fiber arrangement represented by a fundamental block, a horizontal rectangle of finite size. Then the blocks with the same fiber arrangement are repeated infinitely in the vertical direction. In our study the fundamental block is the duct. Since it has rigid boundaries, our infinite fiber arrangement would be built by repeating the fundamental block, using the images method (symmetries with respect to the walls). Contrary to [10], we consider non-penetrable obstacle. But whereas the wave propagation is determined for one particular realization of random fiber arrangement, we perform a statistical average procedure as used in classical multiple scattering theories. Moreover, we consider a larger range of incident wavelength, below the mean distance between scatterers (half the mean distance) and many densities of scatterers.

In section 2 are presented the general scattering problem and the efficient numerical method we have developed to solve it. Extension of this numerical process to compute a coherent field is then detailed. The way the mean amplitudes and the energy transfers are obtained is also clarified. Last, the chosen theoretical models used for comparison with numerical results are presented. Section 3 is devoted to the numerical results obtained by different ways of realizing disorder.

2. Problem formulation

2.1. *Geometry and equations*

An infinite horizontal 2D duct of height h is considered. All lengths of the problem are divided by h, leading to a duct of unitary height $D_\infty = \{(x_1, x_2) \in \mathbb{R}^2; 0 < x_2 < 1\}$ of boundary ∂D_∞. The duct is filled with a compressible fluid and a part D of the duct D_∞, bounded by the vertical boundaries Σ_- at $x_1 = 0$ and Σ_+ at $x_1 = L$, is randomly filled with rigid scatterers (Fig. 1). Finally we note $\Omega_\infty = D_\infty \backslash \mathcal{O}$ the acoustic propagation domain where $\mathcal{O}$ is the union of the interiors of the scatterers and Γ the union of the boundaries of the scatterers. A time harmonic regime of frequency ω is considered. With time dependence $e^{-i\omega t}$

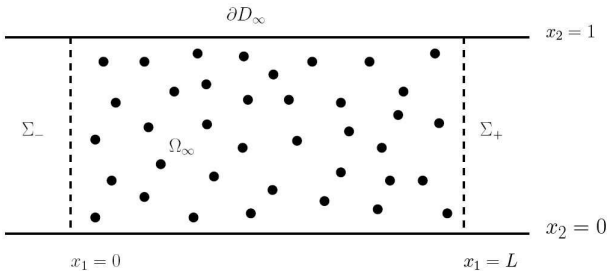

Figure 1. Geometry

omitted, the incident pressure field is noted $p_{inc}(\mathbf{x})$. The total pressure field P reads $P = p_{inc} + p$ where p is the scattered pressure satisfying the equations:

$$\begin{cases} \left(\Delta + k^2\right) p = 0 & \text{in } \Omega_\infty, \\ \dfrac{\partial p}{\partial \mathbf{n}} = -\dfrac{\partial p_{inc}}{\partial \mathbf{n}} & \text{on } \Gamma, \\ \dfrac{\partial p}{\partial \mathbf{n}} = 0 & \text{on } \partial D_\infty, \\ p(\mathbf{x}) = \sum_{n=0}^{\infty} a_n^{\pm} e^{\pm i\beta_n x_1} \theta_n(x_2) \text{ when } x_1 \to \pm\infty \text{ (radiation conditions)} \end{cases} \tag{1}$$

where $\mathbf{n}$ is the exterior normal of Ω_∞ and $k = \omega h/c$ is the dimensionless frequency with c the speed of sound. The radiation conditions are expressed in terms of guided modes defined in appendix A.

2.2. *Numerical method*

We now present the method used to compute efficiently the scattered field. This method has three main advantages: it reduces the infinite domain Ω_∞ to a finite domain Ω of small size, it selects naturally the outgoing solution and it is well-suited for a finite element approximation.

2.2.1. Reduction to a bounded domain

Let us introduce the following integral representation of the scattered pressure field, solution of Eq. 1: $\forall \mathbf{x} = (x_1, x_2) \in \Omega_\infty$:

$$p(\mathbf{x}) = \int_\Gamma \left(p(\mathbf{y}) \, \frac{\partial G(\mathbf{x}, \mathbf{y})}{\partial \mathbf{n}_\mathbf{y}} + \frac{\partial p_{inc}(\mathbf{y})}{\partial \mathbf{n}_\mathbf{y}} \, G(\mathbf{x}, \mathbf{y}) \right) d\Gamma_\mathbf{y}, \tag{2}$$

where $\mathbf{y} = (y_1, y_2)$ and $G(\mathbf{x}, \mathbf{y})$ is the Green's function of the medium without scatterers. The notation $\partial G(\mathbf{x}, \mathbf{y})/\partial \mathbf{n}_\mathbf{y}$ means $\mathbf{n} \cdot \boldsymbol{\nabla}_\mathbf{y} G(\mathbf{x}, \mathbf{y})$. In the free 2D space

the Green's function reads $G(\mathbf{x},\mathbf{y}) = H_0^{(1)}(k|\mathbf{x}-\mathbf{y}|)/4i$ and in the duct case it is the solution of ($\mathbf{y} \in D_\infty$ is supposed fixed):

$$\begin{cases} \left(\Delta_{\mathbf{x}} + k^2\right) G(\mathbf{x},\mathbf{y}) = \delta(\mathbf{x}-\mathbf{y}) & \text{in } D_\infty, \\ \dfrac{\partial p}{\partial \mathbf{n}} = 0 & \text{on } \partial D_\infty, \\ G(\mathbf{x},\mathbf{y}) = \sum_{n=0}^{\infty} g_n^{\pm}(\mathbf{y}) e^{\pm i\beta_n x_1}\theta_n(x_2) \text{ when } x_1 \to \pm\infty. \end{cases}$$

We give in appendix A the expression (modal expansion) of this Green's function and a way to compute it.

2.2.2. Coupling with an integral representation

Now, we present the method to reduce the computation domain. We introduce around each scatterers an artificial boundary. The union of these boundaries is noted Σ (Fig. 2) and the union of the domains between the scatterers Γ and Σ is noted Ω. It is the computation domain and it is chosen small by taking Σ close

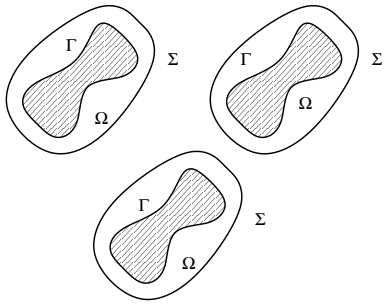

Figure 2. Computational domain

to Γ. The main idea is to use the integral representation (2) to get a boundary condition on the artificial boundary Σ. For $\lambda \in \mathbb{C}$, let us consider the following problem:

$$\begin{cases} \left(\Delta + k^2\right) p = 0 & \text{in } \Omega, \\ \dfrac{\partial p}{\partial \mathbf{n}} = -\dfrac{\partial p_{inc}}{\partial \mathbf{n}} & \text{on } \Gamma, \\ \left(\dfrac{\partial}{\partial \mathbf{n}} + \lambda\right) p(\mathbf{x}) = \left(\dfrac{\partial}{\partial \mathbf{n}} + \lambda\right) \displaystyle\int_\Gamma \left(p(\mathbf{y}) \frac{\partial G(\mathbf{x},\mathbf{y})}{\partial \mathbf{n}_y} \right. & \\ \qquad \left. + \dfrac{\partial p_{inc}}{\partial \mathbf{n}}(\mathbf{y}) G(\mathbf{x},\mathbf{y}) \right) d\Gamma_y & \text{on } \Sigma. \end{cases} \tag{3}$$

Problems (3) and (1) are proved to be equivalent as soon as $\lambda \in \mathbb{C}\backslash\mathbb{R}$ (see [12]).

Remark 1 : If $\Im m(\lambda) = 0$, the problems (3) and (1) are not equivalent for the resonance frequencies k of the interior problem:

$$\begin{cases} \left(\Delta + k^2\right) p = 0 \text{ in } \Omega \cup \overline{\mathcal{O}}, \\ \dfrac{\partial p}{\partial \mathbf{n}} = 0 \text{ on } \Sigma. \end{cases}$$

These resonance frequencies form a sequence $(k_n)_{n\in\mathbb{N}}$ tending to infinity. In particular when Σ is a circle of radius R_Σ, they are the zeros of the first derivative of Bessel functions $J'_m(kR_\Sigma)$, $m \in \mathbb{N}$. When $\Im m(\lambda) \neq 0$ and $k = k_n$, even though problem (3) is well-posed, some instabilities may occur in numerical computations. Better precision can be recovered by adjusting properly $|\Im m(\lambda)|$.

2.2.3. The variational formulation

We note $f = -\partial p_{inc}/\partial \mathbf{n}$ on Γ the source term. The variational formulation of problem (3) is: find $p \in H^1(\Omega) = \left\{p/ \int_\Omega |p|^2 + |\boldsymbol{\nabla} p|^2 < \infty\right\}$ such that ($D_\lambda = \frac{\partial}{\partial \mathbf{n_x}} + \lambda$)

$$\begin{aligned}\int_\Omega \boldsymbol{\nabla} p \cdot \boldsymbol{\nabla} \bar{q} - k^2 \int_\Omega p\bar{q} + \lambda \int_\Sigma p\bar{q} - \int_\Sigma \bar{q}(\mathbf{x}) \int_\Gamma p(\mathbf{y}) D_\lambda \frac{\partial G(\mathbf{x},\mathbf{y})}{\partial \mathbf{n_y}}\, d\Gamma_{\mathbf{y}} d\Sigma_{\mathbf{x}},\\ = \int_\Gamma f\bar{q} - \int_\Sigma \bar{q}(\mathbf{x}) \int_\Gamma f(\mathbf{y}) D_\lambda G(\mathbf{x},\mathbf{y})\, d\Gamma_{\mathbf{y}} d\Sigma_{\mathbf{x}} \text{ for all } q \in H^1(\Omega).\end{aligned}$$

To perform numerical approximation of this formulation, a classic Lagrange finite element method is used. Let $(w_i)_{i=1,N_n}$ be the finite element basis associated to the mesh nodes $(\mathbf{x}_i)_{i=1,N_n}$. We note P_i the approximation of $p(\mathbf{x}_i)$, $F_i = f(\mathbf{x}_i)$ and we define the rigidity matrix and the mass matrices:

$$\mathbb{K}_{ij} = \int_\Omega \boldsymbol{\nabla} w_j \cdot \boldsymbol{\nabla} w_i \text{ and } \mathbb{M}^\Lambda_{ij} = \int_\Lambda w_j w_i \text{ where } \Lambda = \Omega, \Sigma \text{ or } \Gamma.$$

Finally, we introduce the finite element interpolations of the terms involving the Green's function:

$$D_\lambda G(\mathbf{x},\mathbf{y}) \simeq \sum_{k\in I_\Sigma} \sum_{l \in I_\Gamma} \mathbb{N}^S_{kl} w_k(\mathbf{x}) w_l(\mathbf{y}) \text{ and } D_\lambda \frac{\partial G(\mathbf{x},\mathbf{y})}{\partial \mathbf{n_y}} \simeq \sum_{k\in I_\Sigma} \sum_{l \in I_\Gamma} \mathbb{N}^D_{kl} w_k(\mathbf{x}) w_l(\mathbf{y}),$$

where $\mathbb{N}^S_{kl}$ and $\mathbb{N}^D_{kl}$ are the single and double layer matrices:

$$\mathbb{N}^S_{kl} = D_\lambda G(\mathbf{x}_k, \mathbf{y}_l) \text{ and } \mathbb{N}^D_{kl} = D_\lambda \frac{\partial}{\partial \mathbf{n_y}} G(\mathbf{x}_k, \mathbf{y}_l),$$

where I_Σ (resp. I_Γ) is the set of the indexes of the nodes located on Σ (resp. Γ). Thanks to these notations, we are lead to solve the following linear system:

$$(\mathbb{K} - k^2 \mathbb{M}^\Omega + \lambda \mathbb{M}^\Sigma - \mathbb{C}) P = \mathbb{M}^\Gamma F - S,$$

where $\mathbb{C} = \mathbb{M}^\Sigma \mathbb{N}^D \mathbb{M}^\Gamma$ and $S = \mathbb{M}^\Sigma \mathbb{N}^S \mathbb{M}^\Gamma F$.

Remark 2 : As an alternative, an integral equation method [13] could be used with the benefit of a significant mesh size reduction (reduced to Γ). However, compared to such Boundary Element Method (BEM), the method of coupling FEM with an integral representation present the two following advantages: the numerical treatment of the singulatity of the Green's function at $\mathbf{x} = \mathbf{y}$ is avoided and it is easier to extend it to more complicated configurations: impedance boundary condition, penetrable or elastic obstacles. Besides, the maximum cost of the integral representation method lies in the evaluation of the full matrices $\mathbb{N}^S$ and $\mathbb{N}^D$. Such matrices have also to be evaluated with the BEM and are nearly of the same size.

2.3. *Energy balance*

To interpret the numerical results it is useful to use the energy conservation law. For any transverse section Σ of the duct, the energy flux is given by:

$$F(\Sigma) = \int_\Sigma \left(\bar{P} \frac{\partial P}{\partial x_1} - P \frac{\partial \bar{P}}{\partial x_1} \right) dx_2.$$

The energy conservation law expresses as $F(\Sigma_-) = F(\Sigma_+)$. Thanks to the decomposition of the scattered field and total field on the guided modes of the duct (appendix A):

$$\left\{ \begin{array}{l} p(\mathbf{x}) = \displaystyle\sum_{n=0}^{\infty} a_n^r e^{-i\beta_n x_1} \theta_n(x_2) \quad \text{for} \quad x_1 \leq 0, \\ P(\mathbf{x}) = \displaystyle\sum_{n=0}^{\infty} a_n^t e^{i\beta_n (x_1 - L)} \theta_n(x_2) \quad \text{for} \quad x_1 \geq L, \end{array} \right. \tag{4}$$

a simple calculation, for an incident wave as the first guide mode (plane wave) with a unit amplitude $p_{inc}(\mathbf{x}) = e^{ikx_1}$, leads to:

$$F(\Sigma_+) = 2i \sum_{n=0}^{N} \beta_n |a_n^t|^2 \quad \text{and} \quad F(\Sigma_-) = 2i \left(k - \sum_{n=0}^{N} \beta_n |a_n^r|^2 \right),$$

where $N = [k/\pi]$ (the number of propagative modes is $N_p = N + 1$).

Therefore the energy conservation reads $F_{inc} = F_t + F_r$ where $F_{inc} = 2ik$ is the incident energy, $F_t = 2i \sum_{n=0}^{N} \beta_n |a_n^t|^2$ the transmitted energy and $F_r = 2i \sum_{n=0}^{N} \beta_n |a_n^r|^2$ the reflected energy. An alternative writing is $R + T = 1$ with $T = F_t/F_{inc}$ and $R = F_r/F_{inc}$.

2.4. *Application to the determination of an effective equivalent medium*

We have chosen the following numerical procedure: the bounded part D of the duct is filled with N_s scatterers chosen as disks of radius a. We note Φ the scatterers density (or surface fraction). It is defined as the ratio of the surface occupied by the scatterers with the surface $1 \times L$ of D: $\Phi = N_s \pi a^2 / L$.

2.4.1. Mesh generation

To generate a mesh with many scatterers, we first build a reference mesh of an annular region surrounding a scatterer of radius 1 (Fig. 3 (a)), the radius of the exterior circle Σ being 1.5. The interior circle is divided in 16 points and 24 points are used for the exterior circle. A mesh made of two concentric layers of triangles is built in the annular region; it has 80 triangles and 60 vertices.

The procedure to generate a finite element mesh of $N_s = 50$ scatterers and for $L = 2$ consists in dividing D in N_s square cells of size $d = 1/5 (= L/10)$, in choosing the center of the scatterers in each cell following a uniform random law (Fig. 3 (b)) and finally in scaling and translating the reference mesh according to the desired scatterers density. For a mesh of density Φ, the size of the scatterers is $a = \sqrt{\Phi L/(N_s \pi)}$. Since d is fixed, it implies that the disorder becomes weaker when the density increases. To avoid overlaping of scatterers, we prevent the exterior boundary of the reference mesh from exiting the square. This means that the scatterer center is not chosen in a square of size d but of size $d - 3a$. It implies

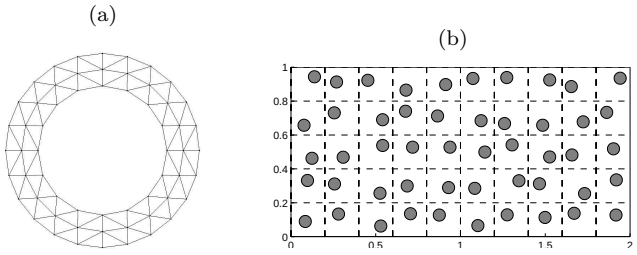

Figure 3. (a): reference mesh (b): random configuration of scatterers for $\Phi = 0.1$

that the exclusion distance between scatterers (the minimal distance between two scatterers) is $3a$ and that the maximum reachable density is $\Phi = 0.35$, obtained for $a = d/3$ (then the union of the scatterers and their surrounding annular regions cover $(1.5)^2 \times 0.35 = 79\%$ of the surface).

Because of the cells subdivision, this is not a complete random realization. It is usually called a perturbed periodic scatterers array. Starting from such array, the random sequential adsorption (RSA) technique might be used to approach a complete disorder [10]. By measuring the radial distribution function (RDF) [2, 10, 14] we have measured the spatial correlation of the scatterers distribution to compare it to the underlying periodic one (Fig. 4). For the periodic case, the RFD

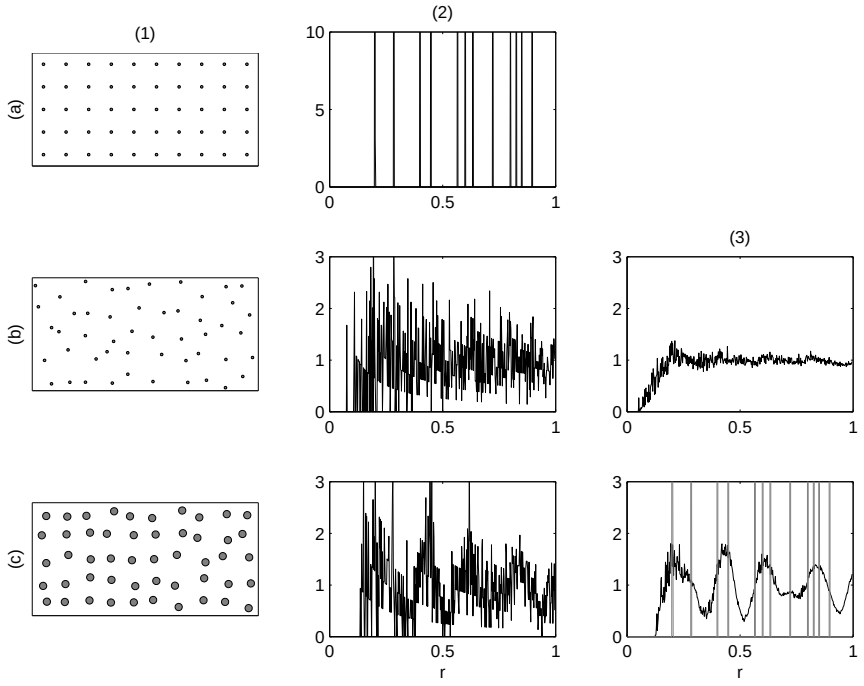

Figure 4. (a): periodic array; (b): perturbed square arrangement $\Phi = 0.01$; (c): $\Phi = 0.08$; (1): scatterers configurations; (2): RFD for one realization; (3): mean RFD for 500 realizations

is characterized by a peaks distribution (Fig. 4 (a)). The RFD of one realization of a perturbed square arrangement is far from this distribution (Fig. 4 (2)). This is also true after averaging on many realizations (Fig. 4 (3b)). Only for rather large densities the RFD reveals oscillations in phase with the peaks distribution of the periodic case (Fig. 4 (c)).

Remark 3 : The computation time is mainly related to the computation of the

terms involving the Green's function (evaluation of series expansion slowly converging and special treatment of singular behavior). For a configuration of 5 scatterers, the computation time is of the order of a few seconds. The computation time varies like N_s^2 and the use of a complete random mesh would imply prohibitive computation times. The advantage of using a perturbed periodic array is to allow to reduce significantly the computations time: the main mesh is divided in ten meshes, each of them corresponding to one vertical slice of the main mesh. For each slice, with typically 5 scatterers, the scattering matrix is computed. Time saving results from the parallelization of the computations and from the ten times reduction of the mesh size. Finally, the scattering matrix of the main layer is obtained from the combination of the ten scattering matrices, with a neglectible computation time.

2.4.2. Computed quantities and mean process

We note N_c the number of random configurations of scatterers taken into account to evaluate the averaged field. For $j = 1$ to N_c, the reflected p_j and transmitted P_j pressure fields are computed in Ω using finite element approximation. The fields $p_j|_{\Sigma_-}$ and $P_j|_{\Sigma_+}$ are computed from the integral representation (2) and the reflection $a_n^{r,j}$ and transmission $a_n^{t,j}$ coefficients defined by Eq. 4 are given by:

$$a_n^{r,j} = \int_0^1 p_j|_{\Sigma_-}\theta_n(x_2)dx_2 \qquad \text{and} \qquad a_n^{t,j} = \int_0^1 P_j|_{\Sigma_+}\theta_n(x_2)dx_2.$$

For the j^{th} pressure field, the reflected energy is $R_j = \sum_{n=0}^N \beta_n|a_n^{r,j}|^2/k$ and the transmited energy is $T_j = \sum_{n=0}^N \beta_n|a_n^{t,j}|^2/k$. They satisfy the conservation law $R_j + T_j = 1$ for $j = 1$ to N_c. The empiric mean fields are defined as:

$$\langle p\rangle(\mathbf{x}) = \frac{1}{N_c}\sum_{j=1}^{N_c} p_j = \sum_{n=0}^{\infty}\langle a_n^r\rangle e^{-i\beta_n x_1}\theta_n(x_2) \quad \text{for} \quad x \le 0,$$

$$\langle P\rangle(\mathbf{x}) = \frac{1}{N_c}\sum_{j=1}^{N_c} P_j = \sum_{n=0}^{\infty}\langle a_n^t\rangle e^{i\beta_n(x_1-L)}\theta_n(x_2) \quad \text{for} \quad x \ge L.$$

To these mean fields are associated the energies of the mean field $\bar{R} = \sum_{n=0}^N \beta_n|\langle a_n^r\rangle|^2/k$ and $\bar{T} = \sum_{n=0}^N \beta_n|\langle a_n^t\rangle|^2/k$. These quantities are different from the mean energies $\langle R\rangle = \sum_{j=1}^{N_c} R_j/N_c = \sum_{n=0}^N \beta_n\langle|a_n^r|^2\rangle/k$ and $\langle T\rangle = \sum_{n=0}^N \beta_n\langle|a_n^t|^2\rangle/k$. Indeed, only the last ones satisfy the energy conservation $\langle R\rangle + \langle T\rangle = 1$.

2.4.3. Models for the transmissions

The mean quantities allow to compute a numerical effective transmission $T_{eff} = |\langle a_0^t\rangle|^2$ that will be compared to transmissions given by analyticial approaches: Foldy's and Linton-Martin's models. They are obtained considering propagation in the free space. They indicate that the mean field is an evanescent plane wave and they link the effective wavenumber of the averaged plane wave to the incident plane wave. Foldy's theory [3] is valid for point scatterers (at least small), far enough from each others (low surface density of scatterers, $a \ll \lambda \ll d$), independent and isotropic. Linton-Martin [6] have extended Foldy's results to the anisotropic case, taking into account pair correlations and calculating the correction of order two in the surface density to Foldy's formula:

$$k_{mod}^2 = k^2 + \delta_1 n_0 + \delta_2 n_0^2 + \cdots, \tag{5}$$

where $n_0 = N_s/L$. This formula is derived assuming small values of the scatterer concentration ($n_0 a^2 \ll 1$ which reads also $a \ll d$) and small values of n_0/k^2 (or equivalently $\lambda \ll d$). At the first order n_0, it is the Foldy's formula. The values of the constants are $\delta_1 = 4i \sum_{n=-\infty}^{\infty} Z_n$ and $\delta_2 = 4\pi i b^2 \sum_{n=-\infty}^{\infty} \sum_{s=-\infty}^{\infty} Z_n Z_s d_{s-n}(kb)$ where $Z_n = J_n'(ka)/H_n'(ka)$, $d_n(x) = J_n'(x)H_n'(x) + [1-(n/x)^2]J_n(x)H_n(x)$ and b is the exclusion distance. In our case $b = 3a$.

To the two model wavenumbers: $k_{Fol}^2 = k^2 + \delta_1 n_0$ and $k_{LM}^2 = k^2 + \delta_1 n_0 + \delta_2 n_0^2$ we associate the transmission coefficients $T_{Fol} = |e^{ik_{Fol}L}|^2$ and $T_{LM} = |e^{ik_{LM}L}|^2$.

3. Numerical results

In all the numerical experiments, we consider a domain of length $L = 2$ and $N_c = 300$ up to 500 configurations. The densities varies from $\Phi = 0.05$ to 0.1 (10% of the surface covered by scatterers) and the incident wavenumber varies between $k = 0.5$ to 60 (dimensionless wavelength $\lambda = 12.6$ to 0.11).

To deal with many parameters is one of the main difficulty of our study. In particular we have three independent distances to consider at the same time: the radius a of the scatterers, the mean distance d between scatterers and the wavelength λ of the incident wave. Once these quantities are fixed, the number N_s of scatterers ($N_s d^2 = L$) and the density of scatterers $\Phi = N_s \pi a^2/L$ are deduced. For a given density there are different ways to create disorder. In order not to change many parameters at the same time to make the interpretation of results easier, we restrict to two ways of mesh generation when Φ varies:

(1) N_s fixed: then $d = \sqrt{L/N_s}$ is fixed and $a = \sqrt{\Phi L/(N_s \pi)}$,
(2) a fixed: then $d = a\sqrt{\pi/\Phi}$ and $N_s = \Phi L/\pi a^2$.

The usual multiple scattering analytical models are generally established for $a \ll \lambda \ll d$. We always consider configurations for which $a \ll \lambda$ and $a \ll d$, but we do not restrict to $\lambda \ll d$. We consider the larger range $\lambda/d = 0.5$ to 63. In the two following subsections we fix $N_s = 50$ and therefore $d = 0.2$.

3.1. *Influence of the frequency*

We consider a moderate density $\Phi = 0.04$ which corresponds to scatterers of size $a = 0.023$. The frequency k varies from 0.5 to 60 which corresponds to $\lambda/d = 0.5$ to 62.8.

3.1.1. Energy transfers

On Fig. 5 (a) is represented the mean transmitted energy $\langle T \rangle$ versus the frequency. We have observed that $\langle R \rangle + \langle T \rangle = 1$ with a good precision except the occurence of a numerical instability for the frequency $k = 54.5$, where a peak can also be seen on Fig. 5 (a) : this is a resonance frequency described in remark **1**. The first zero of $J_1'(z)$ is in $z = 1.84$ leading to $k_{res} = 54.4$ ($R_\Sigma = 1.5a$). On Fig. 5 (a) is seen that for small frequencies the mean transmitted energy $\langle T \rangle \simeq 1$: the wavelength is so long that the scatterers are "transparent" and all the injected energy is transmitted. For large frequencies, scattering effects are strong and most of the mean energy is reflected ($\langle R \rangle = 1 - \langle T \rangle \simeq 0.7$ for $k = 60$). On Fig. 5 (b) we get that the total energy of the mean field satisfies $\bar{R} + \bar{T} < 1$ because of the loss of energy through the averaging process. More precisely $\langle T \rangle$ measures the transmitted energy of the whole field while $\bar{T}$ measures the transmitted energy of the coherent field. Thus $\langle T \rangle - \bar{T}$ measures the transmitted energy of the incoherent field. Excepting

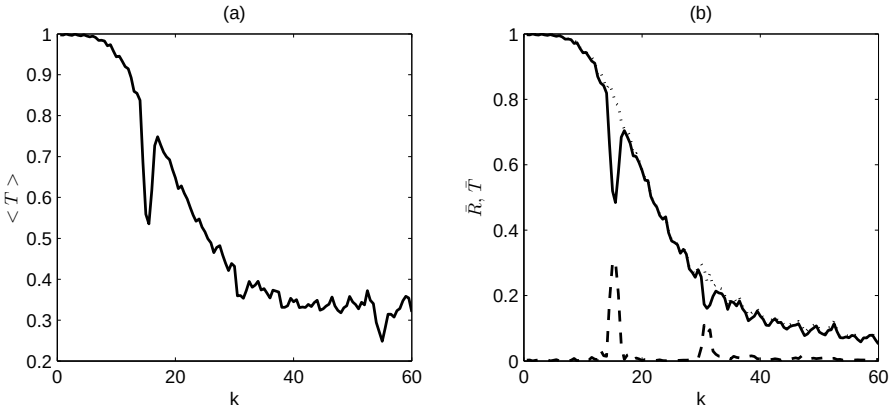

Figure 5. $\Phi = 0.04$; (a): $\langle T \rangle$ versus k; (b): solid line: $\bar{T}$, dashdot: $\bar{R}$, dot: $\bar{R} + \bar{T}$

around the frequencies $k = 15.5$ and $k = 30.5$ (see explanations latter) we obtain $\bar{R} \simeq 0$ which indicates that the mean field is essentially transmitted.

To go further, we have determined how the energy is distributed over the modes of the duct. The reflected and transmitted energy can be decomposed on the guided modes: for example one gets $\langle R \rangle = \sum_{n=0}^{N} \langle R \rangle_n$ where $\langle R \rangle_n = \beta_n \langle |a_n^r|^2 \rangle / k$. This is the mean reflected energy carried by the n^{th} propagative mode. We have found that the mean reflected energy is carried by all the propagative modes whereas the mean transmitted energy is mainly carried by the plane mode. In a same way, only the plane mode is involved in the energy of the mean field: $\bar{R} \simeq \bar{R}_0 = |\langle a_0^r \rangle|^2$ and $\bar{T} \simeq \bar{T}_0 = |\langle a_0^t \rangle|^2$. In other words, the mean field is a plane wave, as assumed in theoretical models.

The peaks observed on Fig. 5 (a) and (b) at $k = 15.5$ and $k = 30.5$ correspond to some of the band gap frequencies of the "underlying" periodic array ($N_s = 50$ scatterers located at the middle on the square cells). Band gap frequencies of the

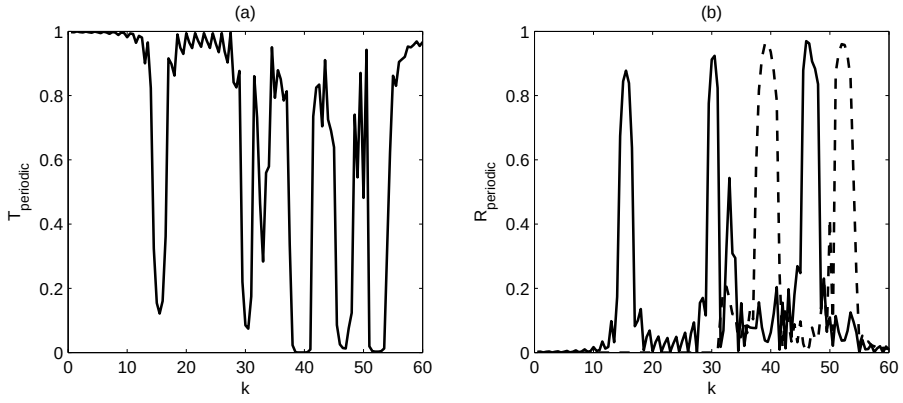

Figure 6. (a) Transmission and (b) reflection (solid line :mode 0, dot : mode 10) in a periodic array

periodic array are shown on Fig. 6: they correspond to a drop of the transmission or a maximum of the reflection when sending a plane wave on the periodic array. Only modes 0, 10, 20, $\cdots$ can be produced by an incident plane wave. Indeed, due to some properties of the the geometry and of the data, both symmetrical about the midline $y = 1/2$ and vertically periodic with 5 periodicity cells, we can prove by constructing explicit solutions and by a uniqueness argument that the scattered field expands only on the modes of orders $n = 2 \times 5 \times p$, $p \in \mathbb{N}$. Of course this argument fails once disorder is introduced. On Fig. 6 (b) are represented separately the reflections of mode 0 (solid line) and of mode 10 (doted line). Mode 10 becomes

propagative for $k \geq 31.5$ ($10\pi = 31.4$) and mode 20 for $k \geq 60$. Modes 0 and 10 behave differently and two kind of band gaps exist. First the ones associated with a strong reflection of the mode 0 ($k = 15.5$, 30.5 and 47). They correspond respectively to $\lambda = 2d$, d and $2d/3$. Therefore they agree with the law $kd = n\pi$, n integer, for a one-dimensional periodic array [15]. This law is usually no longer valid in a 2D periodic array [15] and thus seems to extend to 2D arrays in ducts for plane mode propagation. The other band gap family corresponds to a strong reflection of the mode 10 ($k = 40$ and 52). On Fig. 5 (b), only the low frequency band gaps of the plane mode $k = 15.5$ and 30.5 are seen. We do not observe any drop behavior of $\bar{T}$ at the larger band gap frequencies $k = 40$, 47 and 52, but notice that $\bar{T}$ is too small to be clearly interpreted above $k = 31.5$.

It could have been expected that an averaged perturbed periodic array would behave like a periodic array. Comparison of the transmission in the perturbed (Fig. 5 (b)) and unperturbed periodic array (Fig. 6 (a)) contradicts this expectation. For the frequencies outside the fondamental band gaps, $\bar{T}$ and $T_{periodic}$ are completly different and, as we will see latter, only $\bar{T}$ obeys a multiple-scattering law. On the contrary, for frequencies in the fondamental band gaps below the cut-off of the 10^{th} guided mode, we recover the behavior of the periodic array. The influence of the periodic band gaps would probably disappear in case of complete randomness as suggested by [10] in the case of one realization.

3.1.2. Effective transmissions

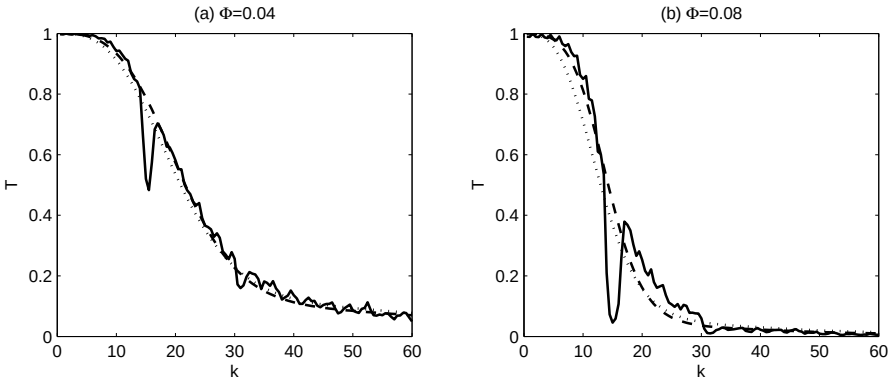

Figure 7. solid line: numerical values, dot: Foldy, dash: LM

On Fig. 7 (a) the numerical transmission is compared to the theoretical transmissions versus the frequency. Good accordance is found excepting for the band gap frequencies $k = 15.5$ and 30.5. It is not possible to decide which model, Foldy or LM, is closer from numerical experiments. On Fig. 7 (b) are represented the same quantities for a larger density $\Phi = 0.08$. As expected, the numerical values go away from the model ones when the density increases. Moreover the drops of the numerical transmission at the band gap frequencies are amplified, because the perturbation of the periodic array is less random for larger densities. Note that LM model seems to be more suited than Foldy's model for low frequencies.

3.2. *Influence of the density*

Now, the frequency k is fixed and we study the influence of the density $\Phi = 0$ to 0.1 which corresponds to scatterers sizes $a = 0.008$ to 0.036. We have studied the case of an incident wave with λ varying from $3d$ to $d/2$ (Fig. 8). A general observation

is that for all frequencies, the difference between T_{eff} and T_{mod} ($mod = Fol$ or LM) is very small for small densities.

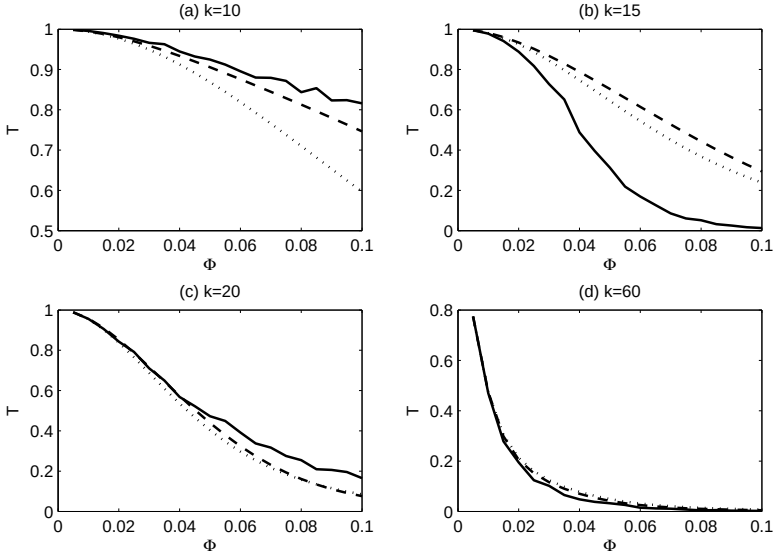

Figure 8. $\Phi = 0.04$; solid line: numerical values, dot: Foldy, dash: LM

In the case $k = 10$ ($\lambda = 3d$) is found that the attenuation in a duct is weaker than the attenuation predicted by models derived in the free space. It is due to the guided effect of the duct. Foldy's model predicts to much attenuation and T_{LM} is the closest from T_{eff}. For the case $k = 15$ ($\lambda = 2d$), agreement between numerical and theoretical results is very poor. As already mentioned, this is because we are close from a band gap frequency of the periodic array and it is not a multiple scattering regime. At last, for small wavelengths $k = 20$ to $k = 60$ (then $\lambda = d/2$), Fig. 8 shows good accordance between numerical effective wavenumber and theoretical models developed in the free space. This means that in a duct guided effects are weaker than multiple-scattering effects.

3.3. *Other configurations*

Finally, in this section, we consider other ways to create random configurations: by reducing the mean distance d, by increasing the number of scatterers N_s or by changing the scatterers shape.

3.3.1. Case $d = 0.1$

We have studied the influence of halving the mean distance $d : 0.2 \to 0.1$. Then the scatterers size is reduced $a \to a/2$ and the number of scatterers increases $N_s \to 4N_s = 200$ (20×10 scatterers). In the free space, multiple scattering is invariant by scaling: when all the distances of the problem, d, λ and a, are halved, the multiple scattering effects are the same. In particular for the models wavenumbers, applying the scaling $k \to 2k$ (since $\lambda \to \lambda/2$) in Eq. 5 leads to $k_{mod} \to 2k_{mod}$ (and thus $k_{mod}d$ constant). Therefore in the free space, the two pertinent non-dimensional parameters are the density $\Phi = \pi(a/d)^2$ and d/λ (or kd). The numerical experiments (for $d = 0.1$ and $k = 20$, $k = 30$ and $k = 40$) in a duct show the same behavior. In other words, the number of scatterers in a vertical section of the duct does not influence significantly the values of the effective parameters.

3.3.2. Case of a fixed scatterers size

When the size of the scatterers $a = 0.01$ is fixed ($d = a\sqrt{\pi/\Phi}$ varies from 0.25 to 0.05) we can still assume we are mostly in the regime $a \ll d$. The number of scatterers N_s varies in a large range from 32 to 648 and for large values of N_s time computations become very long. Fig. 9 shows an example of arrangement and the associated RFD for $\Phi = 0.04$ ($N_s = 23 \times 11 = 253$). One advantage to work with

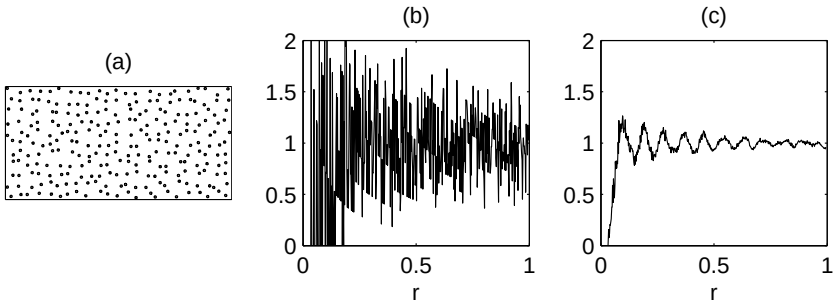

Figure 9. (a): perturbed square arrangement for $\Phi = 0.04$; (b): RFD for one realization; (3): mean RFD for 500 realizations

a fixed size of scatterers is that the step of the mesh, and thus the finite element error, is fixed when k or ϕ vary. The conclusion is the same than in the previous paragraph: the values of the effective transmission just depends on the value of kd. The results obtained for a frequency k and a distance $d = a\sqrt{\pi/\Phi}$ are the same than the results associated to $d' = 0.2$ (for instance) and a frequency k' such that $kd = k'd'$.

3.3.3. Extension to square scatterers

Our numerical method extends naturally to any scatterers shape, for example squares. Only the reference mesh has to be changed and it is represented on Fig. 10 (a). To a random location in each cell, a random rotation is applied to the squares (see an example on Fig. 10 (b)). From the curve of the transmission versus the

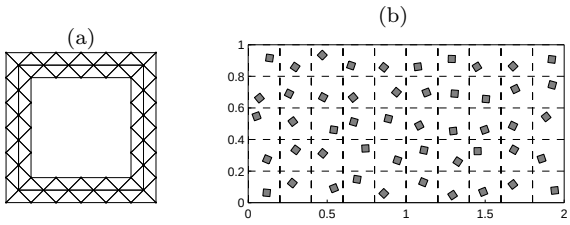

Figure 10. (a): reference mesh, (b): example of a random configuration

frequency for $\Phi = 0.08$ (Fig. 11), we observe behaviors similar to those for circular scatterers. In particular at the band gap frequencies the transmission vanishes. T_{eff} is farther from T_{mod} than in the disks case (same density), but such models have been developed for circular obstacles. After the second band gap at $k = 30.5$, T_{eff} nearly vanishes whereas it was small for disks configuration because of stronger scattering effect of squares corners.

4. Conclusion

We have developed a numerical approach to determine the effective properties of a random medium in a duct. The choice of a FEM method allows to consider

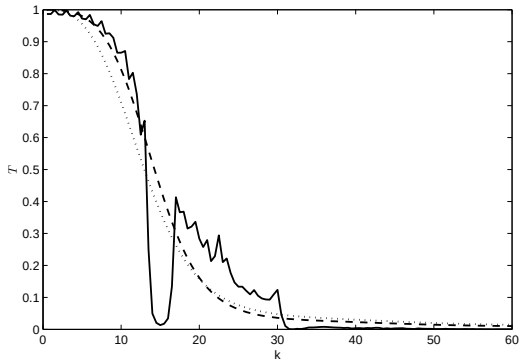

Figure 11. $\Phi = 0.08$; solid line: numerical values, dot: Foldy, dash: LM

scatterers of arbitrary shapes whereas the coupling of FEM with an integral representation, based on the duct Green's function, allows to reduce significantly the mesh size. Time saving is also obtained by considering a perturbed periodic array for the scatterers positions instead of complete randomness: the scatterers are placed on a reference periodic array and are moved locally randomly.

We have shown that the effective medium is well described by analytical models, Foldy's and Linton-Martin models, although they are not designed for a duct configuration, except for the lowest band gap frequencies of the reference periodic array. In that case, the effective medium behaves like a periodic one.

Appendix A. Green's function of a guide

It is convenient to define the Green's function of the duct thanks to the duct mode i.e. the solution $p(x_1, x_2)$ of Helmholtz equation in the duct with Neuman boundary condition on the rigid walls and with separated variables $p(x_1, x_2) = \theta(x_2)e^{i\beta x_1}$. The transverse modes read for all $n \in \mathbb{N}$:

$$\theta_n(x_2) = \sqrt{2 - \delta_{n0}}\cos(n\pi x_2)$$

and define an orthonormal basis of $L^2(]0,1[)$. The wavenumbers β_n are given by:

$$\beta_n = \sqrt{k^2 - (n\pi)^2} \quad \text{if} \quad n \leq \frac{k}{\pi} \quad \text{and} \quad \beta_n = i\sqrt{(n\pi)^2 - k^2} \quad \text{if} \quad n > \frac{k}{\pi}.$$

A real β_n corresponds to a propagative mode and an evanescent mode is associated to a complexe β_n. It is straightforward to determine the Green's function of the duct as a modal expansion [16]:

$$G(\mathbf{x}, \mathbf{y}) = \sum_{n=0}^{\infty} \frac{e^{i\beta_n|x_1 - y_1|}}{2i\beta_n}\theta_n(x_2)\theta_n(y_2). \tag{A1}$$

Note that the Green's function is not defined if there exists n such that $\beta_n = 0$. This happens for the sequence of the cut-off frequencies of the duct $k \in \{k_n = n\pi, n \in \mathbb{N}\}$. In practice we avoid these frequencies. It is convenient to write the Green's function as

$$G(\mathbf{x}, \mathbf{y}) = \frac{e^{ik|x_1 - y_1|}}{2ik} + \sum_{n=1}^{\infty} G_n \text{ where } G_n = \frac{e^{i\beta_n|x_1 - y_1|}}{i\beta_n}\cos(n\pi x_2)\cos(n\pi y_2).$$

As G_n has the following asymptotic behavior:

$$G_n \underset{n\to\infty}{\sim} -\frac{e^{-n\pi|x_1-y_1|}}{n\pi}\cos(n\pi x_2)\cos(n\pi y_2),$$

the expansion (A1) is semi-convergent when $|x_1 - y_1| = 0$ and converges slowly when $|x_1 - y_1|$ is small (weak exponential decay). A classical way [16] to recover a fast convergent series is to extract the singular part of $\tilde{G} = \sum_{n=1}^{\infty} G_n$:

$$S(\mathbf{x},\mathbf{y}) = -\sum_{n=1}^{\infty}\frac{e^{-n\pi|x_1-y_1|}}{n\pi}\cos(n\pi x_2)\cos(n\pi y_2).$$

This expansion S is still semi-convergent but has an exact analytical expression:

$$S(\mathbf{x},\mathbf{y}) = \frac{1}{4\pi}\ln\Big\{4e^{-2\pi|x_1-y_1|}\left[\cosh(\pi|x_1-y_1|)-\cos(\pi(x_2+y_2))\right], \\ \times\left[\cosh(\pi|x_1-y_1|)-\cos(\pi(x_2-y_2))\right]\Big\}.$$

Finally we define the "residual" part which has a better convergence:

$$R(\mathbf{x},\mathbf{y}) = \tilde{G}(\mathbf{x},\mathbf{y}) - S(\mathbf{x},\mathbf{y}) = \sum_{n=1}^{\infty}\left(\frac{e^{i\beta_n|x_1-y_1|}}{i\beta_n} + \frac{e^{-n\pi|x_1-y_1|}}{n\pi}\right)\cos(n\pi y_2),$$

such that $G = (e^{ik|x_1-y_1|}/2ik) + S + R$. When $|x_1 - y_1| = 0$, the terms of the expansion behave like n^{-3}. Thanks to this fast convergence, only a few term in the sum are necessary to get a good approximation of the Green's function. In practice the number of term taken into acount is chosen such that the error is less than 1%.

References

[1] M. Chekroun, L. Le Marrec, B. Lombard, J. Piraux and O. Abraham, *Comparison between a multiple scattering method and direct numerical simulations for elastic wave propagation in concrete*, Ultrasonic Wave Propagation in Non Homogeneous Media, Series: Springer Proceedings in Physics, 128 (2008), A. Leger, M. Deschamps (Eds.) pp. 317–327.

[2] A. Derode, V. Mamou, A. Tourin, *Influence of correlations between scatterers on the attenuation of the coherent wave in a random medium*, Phys. Rev. E 74 (2006), id. 036606.

[3] L.L. Foldy, *The multiple scattering of waves. I: General Theory of isotropic scattering by randomly distributed scatterers*. Physical Review. 67 (1945), pp. 107–119.

[4] V. Twersky, *On Scattering of Waves by Random Distributions. I. Free-Space Scatterer Formalism*, J. Math. Phys. 3 (1962), pp. 700–715.

[5] B.C. Gupta and Z. Ye, *Localization of classical waves in two-dimensional random media: A comparison between the analytic theory and exact numerical simulation*, Physical Review E 67 (2003), id. 036606.

[6] C.M. Linton and P.A. Martin, *Multiple scattering by random configurations of circular cylinders: Second-order corrections for the effective wavenumber*, J. Accoust. Soc. America 117 (2005), pp. 3413–3423.

[7] K. Nakashima, S. Biwa and E. Matsumoto, *Elastic Wave Transmission and Stop Band Characteristics in Unidirectional Composites*, J Journal of Solid Mechanics and Materials Engineering 2 (2008), pp. 1195–1206.

[8] J. Segurado and J. Llorca, *A numerical approximation to the elastic properties of sphere-reinforced composites*, Journal of the Mechanics and Physics of Solids 50 (2002), pp. 2107–2121.

[9] N.A. Gumerov and R. Duraiswami, *Computation of scattering from clusters of spheres using the fast multipole method*, J. Acoust. Soc. Am. 117 (2005), pp. 1744–1761.

[10] S. Biwa, F. Kobayashi and N. Ohno, *Influence of disordered fiber arrangement on SH wave transmission in unidirectional composites*, Mechanics of Materials 39 (2007), pp. 1–10.

[11] R.-B. Yang and A.K. Mal, *Multiple scattering of elastic waves in a fiber-reinforced composite*, J. Mech. Phys. Solids 42 (1994), pp. 1945–1968.

[12] A. Jami and M. Lenoir, *A variational formulation for exterior problems in linear hydrodynamics*, Comput. Method Appl. Mech. Engrg. 16 (1978), pp. 341–359.

[13] W.L. Wendland, *Boundary Element Topics*, Springer (1995).

[14] R. Pyrz, *Correlation of microstructure variability and local stress field in two-phase materials*, Mater. Sci. Eng. A177 (1994), pp. 253-259.
[15] F. Kobayashi, S. Biwa and N. Ohno, *Wave transmission characteristics in periodic media of finite length: multilayers and fiber arrays*, Int. J. Solids Struct. 41 (2004), pp. 7361–7375.
[16] R.E. Collin, *Field theory of guided waves*, IEEE Press (1991), pp. 78–86.